Journal of Alloys and Compounds 511 (2012) 139–143

Contents lists available at SciVerse ScienceDirect

Journal of Alloys and Compounds

journal homepage: www.elsevier.com/locate/jallcom

Crystal structure, magnetic properties and ESR spectra of $Ca_3Co_{2-x}Fe_xO_6$

J. Chen, Z.W. Ouyang*, N.M. Xia, S.S. Sheng, Y.Y. Wu, Z.C. Xia, L. Li

Wuhan National High Magnetic Field Center, Huazhong University of Science and Technology, Wuhan 430074, People's Republic of China

ARTICLE INFO

Article history:
Received 5 May 2011
Received in revised form 10 August 2011
Accepted 4 September 2011
Available online 10 September 2011

PACS:
75.30.Kz
76.30.–v
74.62.Bf

Keywords:
Spin-chain compound
Crystal structure
Magnetization
ESR spectra

ABSTRACT

We have synthesized compounds of $Ca_3Co_{2-x}Fe_xO_6$ ($x = 0$–1.5) by sol–gel reaction method. X-ray diffraction data show that the solubility limit of Fe in the spin-chain compound $Ca_3Co_2O_6$ is about $x = 0.7$. For the rhombohedral ($R\bar{3}c$) samples with $x \leq 0.7$, the upward deviation from the paramagnetic Curie–Weiss law in the inverse magnetic susceptibility (H/M) tends to be suppressed at $x = 0.7$. Correlatively, the paramagnetic Curie temperature θ_P approaches zero at this concentration. The $M(H)$ curves exhibit a well-defined ferrimagnetic state, which becomes smeared out with increasing Fe concentration and nearly disappears at $x = 0.7$. For the triclinic ($P\bar{1}$) samples with $x = 1.1$, the magnetization is much small and its ground state is antiferromagnetic. The H/M curve measured up to 300 K does not follow the Curie–Weiss law. Finally, ESR spectra composed of eight hyperfine splittings due to Co nuclear spin are observed for $x = 0.4$.

1. Introduction

For more than 10 years, quasi-one-dimension (1D) spin-chain compounds $Ca_3(Co, T)_2O_6$ (T = transition metal ions) have been attracting a lot of interests due to their anisotropic magnetic properties [1–7]. The parent compound $Ca_3Co_2O_6$ crystallizes in K_4CdCl_6-type crystal structure (space group $R\bar{3}c$), in which face-sharing CoO_6 octahedra (Co_1) and CoO_6 trigonal prisms (Co_2) are aligned alternately, forming spin chains along the crystallographic c axis [8]. These linear chains are arranged triangularly in the ab plane with ferromagnetic (FM) intrachain interaction being much larger than antiferromagnetic (AFM) interchain interaction [1,8–10]. The Ising-like chains along with the AFM interchain coupling introduce geometric magnetic frustration, giving rise to interesting magnetic properties such as spin freezing and partially disordered AFM (PDA) state, where 2/3 of the chains are coupled antiferromagnetically while 1/3 is left disordered [9]. To better understand the unusual properties of this compound, many efforts have been made to tune the intrachain and interchain interactions by a suitable substitution at the Co site of $Ca_3Co_2O_6$ [2,3,11–14].

In recent years, Jain et al. [14,15] reported the crystal structure and magnetic properties of $Ca_3Co_{2-x}Fe_xO_6$ with $x = 0$–0.4 and 1.0. It was found that Fe doping leads to a breaking of the FM linear spin chains and simultaneously introduces AFM exchange interaction between Fe^{3+} irons. Recent neutron diffraction experiments [16] of $x = 0.2$ and 0.4 have demonstrated two different magnetic structures, amplitude modulated structure with a propagation vector $K = (0, 0, 1)$ and PDA structure with $K = (0, 0, 0)$, details of which cannot be distinguished. No transition from PDA to ferrimagnetic (FIM) state was found. Recalling that a FIM state has been observed in the Cr- and Mn-doped compounds [13,17], where both Cr and Mn tend to suppress the intrachain FM coupling and enhance the AFM coupling, it is expected that a similar FIM state exists in the Fe-doped compounds. In addition, the Fe-doped compounds reported earlier [14–16] were synthesized by traditional solid state method and no solubility limit was found. Compared to the solid state method, the sol–gel reaction method can achieve a mixture on the atomic level of the components, leading to a better crystallization. In this paper, we perform a systematic study on crystal structure and magnetic properties of Fe-doped compounds within $x = 0$–1.5, a concentration range much larger than that adopted in Refs. [14–16]. We find that the rhombohedral structure survives up to $x = 0.7$, which was not found before. Unusual and interesting magnetic properties are observed. We also note that Kageyama et al. [18] carried out an ESR study of $Ca_3Co_{1.98}Fe_{0.02}O_6$ and observed successfully an isolated electron state of Fe^{3+} with $g = 2.0$. This urges us to examine the ESR spectra of the present compounds with larger Fe concentration. As a result, a resonance of Co ions, rather than that of Fe ions, is observed.

* Corresponding author.
E-mail address: zwouyang@mail.hust.edu.cn (Z.W. Ouyang).

0925-8388/$ – see front matter © 2011 Elsevier B.V. All rights reserved.
doi:10.1016/j.jallcom.2011.09.010

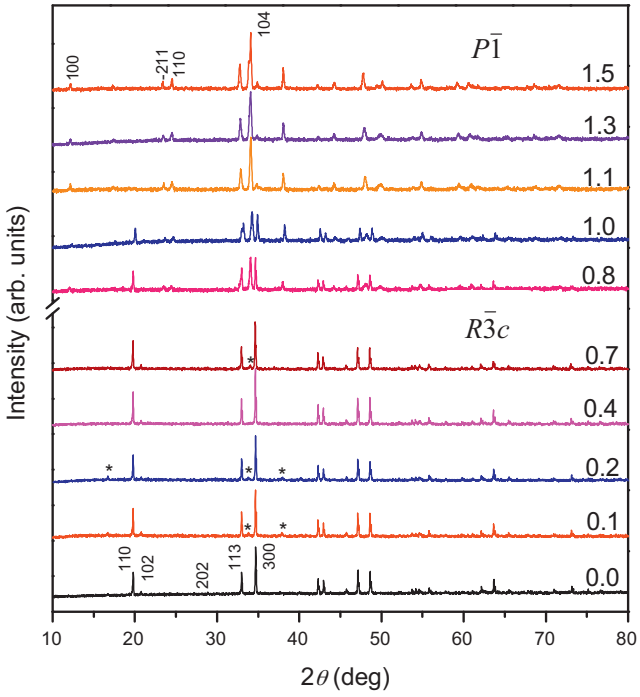

Fig. 1. Room temperature XRD patterns of $Ca_3Co_{2-x}Fe_xO_6$ (x = 0–1.5). The impurity peaks are marked by asterisks.

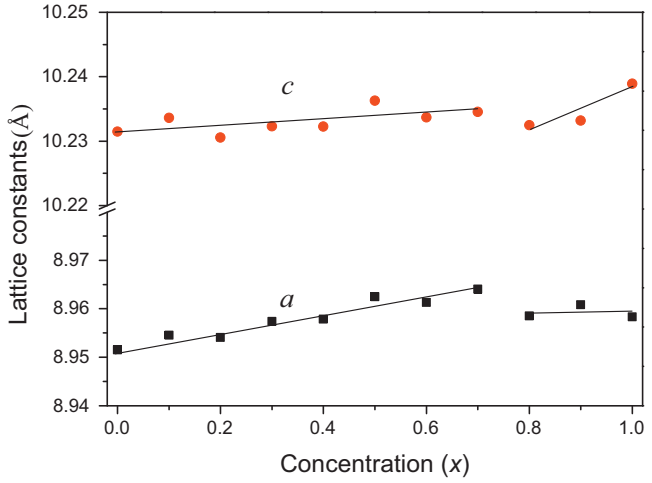

Fig. 2. Fe concentration dependence of the lattice constants. The solid lines are guides to the eyes.

2. Experimental

Polycrystalline samples of $Ca_3Co_{2-x}Fe_xO_6$ (x = 0.1–1.5) were prepared by sol–gel reaction method. The required reagents $Ca(NO_3)_2$, $Co(NO_3)_2$ and $Fe(NO_3)_3$, each with a purity of 99.99%, were dissolved in alcohol, to which concentrated nitric acid and citric acid were subsequently added for sol formation. The solution was gradually heated at 70 °C in the heating blender for evaporation and became into the gel form. The gel was dried in vacuum drying oven for 24 h. The dried gel was then calcined at 700 °C for 2 h and subsequently heated at 850 °C for 24 h with intermediate grindings. Room temperature X-ray powder diffraction (XRD) data were collected by an X'pert diffractometer with Cu Kα radiation. The magnetization measurements were performed in a superconducting quantum interference device magnetometer over a temperature range of 2–300 K and a magnetic field range of 0–7 T. Before each measurement, the sample was zero-field cooled (zfc) from paramagnetic (PM) state at 300 K to the desired temperature. The ESR measurements of x = 0.4 were performed using a Bruker X-band (9.4 GHz) spectrometer within a temperature range of 2–300 K.

3. Results and discussion

3.1. Crystal structure

Fig. 1 shows XRD patterns for some representative compounds. For x = 0 (i.e., $Ca_3Co_2O_6$), the main low-angle peaks (1 1 0), (1 1 3) and (3 0 0) for the rhombohedral structure (space group $R\bar{3}c$) are clearly visible and no second phase is detected. With the increase of Fe concentration, several additional peaks labeled by asterisks in the figure appear except for sample with x = 0.4, which still owns a pure phase. As x is increased to 0.8, the impurity peak located in between the (1 1 3) and (3 0 0) peaks becomes stronger and (1 1 0) peak becomes weaker in intensity, accompanied by a widening of (1 1 3) peak and an appearance of additional peaks at low angles. This shows that a considerable amount of secondary phase develops in the specimen. Further increasing x to 1.1, the (1 1 0) peak disappears completely. All the XRD patterns of x = 1.1–1.5 can be indexed in the triclinic structure (space group $P\bar{1}$) with low-angle peaks marked in Fig. 1, in agreement with the previous report on x = 1.0 (i.e., Ca_3CoFeO_6) [15]. Note that space group $P\bar{1}$ owns a very low symmetry and it is not possible to determine the structural details by Rietveld refinement because the initial positions of the atoms in the unit cell are not available in the literature [15]. Despite this deficiency, our XRD data shows that the dominant phase for samples with x = 0–0.7 is the rhombohedral structure, whereas that for x = 1.1–1.5 is the triclinic structure. In the intermediate range of concentration, x = 0.8–1.0, the samples contain both phases. The lattice constant as function of x for the rhombohedral phase is shown in Fig. 2. Both a and c for $x \leq 0.4$ are found to be smaller approximately by ~1.4% than those of samples synthesized by solid state method [14]. This might be due to either zero-point shift of the diffractometer or oxygen defects existing in the compounds. Fig. 2 also reveals a slight increase of both a and c for $x \leq 0.7$, although there is a small fluctuation caused probably by chemical composition deviation during the materials synthesis process. For x = 0.8–1.0, the x dependence of lattice constant presents a different behavior. This suggests that the solid solubility of Fe in $Ca_3Co_2O_6$ is about 0.7 for rhombohedral phase, in accordance with the XRD patterns shown in Fig. 1. Table 1 gives the lattice constants of compounds with x = 1.1–1.5. No dramatic changes are found except for a small fluctuation.

3.2. Magnetic properties

The samples with x = 0.1, 0.2 and 0.7 contain a small amount of secondary phase, probably the triclinic phase (see Fig. 1) with much week magnetization (see below). Thus, the magnetization contribution from the secondary phase can be ignored. Differences of magnetic properties for samples with both phases are clearly illustrated in Fig. 3 for x = 0.7 ($R\bar{3}c$) and x = 1.1 ($P\bar{1}$). The $M(T)$ curves for x = 0.7 are quite similar to those of x = 0–0.4 reported earlier [14]. The zfc heating $M(T)$ curve presents an anomaly at ~5 K, characterizing a transition from FIM (or AFM) to PM state. The fc cooling curve branches from the zfc heating one at low temperature due to the geometrical frustration of triangular lattice [14]. The inverse magnetic susceptibility (H/M) shown in the inset of Fig. 3a obeys the Curie–Weiss law with μ_{eff} = 5.6 μ_B/f.u. and θ_P = 0 K. This implies

Table 1
Lattice constants (Å and°) of $Ca_3Co_{2-x}Fe_xO_6$ (x = 1.1–1.5) with triclinic phase.

x	a	b	c	α (°)	β (°)	γ (°)
1.1	8.0038	5.7029	12.5536	73.2781	103.4907	113.1429
1.2	8.0098	5.6920	12.5418	73.2677	103.5374	113.2586
1.3	8.0145	5.7159	12.5746	73.2795	103.4317	113.2061
1.4	8.0168	5.7129	12.5694	73.2795	103.4126	113.2468
1.5	8.0106	5.7080	12.5646	73.3196	103.3577	113.1972

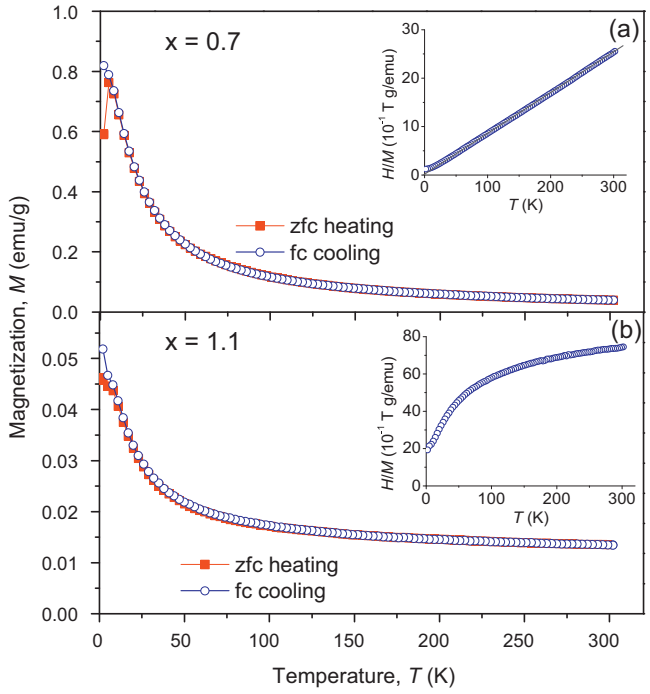

Fig. 3. $M(T)$ curves measured in 0.1 T for $x = 0.7$ and 1.1. The insets show the H/M curves. The solid line represents Curie–Weiss fits.

that $x = 0.7$ is quite unusual and there exists a strong competition between FM and AFM interactions at this concentration. To explore the details, we show in the inset of Fig. 4 the H/M vs. T curves for $x \leq 0.7$. The high-temperature curve complies well with the Curie–Weiss law, while the low-temperature part does not but exhibits an upturn due to the presence of short-range ordering. This upturn becomes ambiguous as x increases and almost disappears at $x = 0.7$. Simultaneously, the value of θ_P decreases and eventually reaches zero because the intrachain FM coupling (J) is reduced. It was reported that J can be determined by the expression $\chi T = 3/4\, g^2 \exp[(8J/k_B T)]$, where χ is the molar susceptibility, for $S = 2$ one-dimensional Ising spin chain [13,19]. It can be seen from Fig. 4 that the value of χT for $x = 0.0$ increases as temperature decreases from 300 K. This will yield a positive J value if the

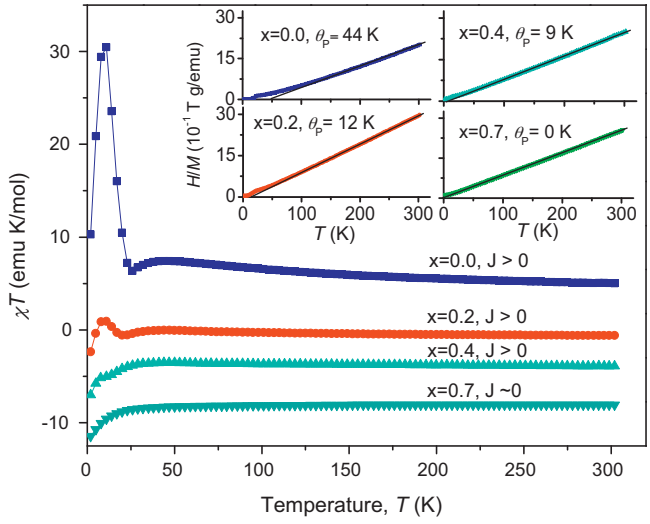

Fig. 4. χT vs. T curves for $x \leq 0.7$. For $x = 0.2$, 0.4 and 0.7, the χT values are shifted down by 4, 8 and 12 (emu K/mol), respectively. The inset shows the H/M vs. T curves. The solid lines represent Curie–Weiss fits.

high-temperature curve is fitted using the expression above (the present system is a mixed system with $S = 2$ (Co^{3+}) and $S = 5/2$ (Fe^{3+}) [14], which prevents us from obtaining the exact J value). This feature is gradually suppressed with increasing x and the high-temperature χT curve nearly becomes a horizontal line at $x = 0.7$, yielding a value of $J = 0$. Thus, there exists an intimate correlation between the upturn of H/M and θ_P (J). Note that in the precious report [14], it was at $x = 0.4$ that the θ_P starts to become negative. This shows that the intrachain FM interaction is stronger in present samples as compared with those of Ref. [14] probably because of the differences in sample-synthesis conditions. We also note that $x = 0.7$ associated with magnetic anomalies points to the solubility limit of Fe in the rhombohedral phase. Thus, it is likely that crystallographic structure correlates with the competing FM and AFM interactions.

In comparison to $x = 0.7$, the $M(T)$ curves for $x = 1.1$ (Fig. 3b) show some different behaviors: (1) the magnetization is much smaller and the anomaly observed at ~7 K might characterize an AFM transition; (2) the high-temperature magnetization is unusually large compared with the low-temperature region, although the curve exhibits a PM-like behavior; (3) the H/M curve shown in the inset of Fig. 3b does not follow the Curie–Weiss law. These indicate that the ordering temperature of this compound might be higher than 300 K or there exist short-range FM correlations in the PM matrix. It is worth noting that no spin reorientation is observed at ~193 K for the present sample with $x = 1.1$, different from the isostructural sample with $x = 1.0$ [15].

Differences in magnetic properties for both structures are also manifested in the $M(H)$ curves shown in Fig. 5. For $x = 0.2$, the magnetization at 2 K presents a large hysteresis between the H-increasing and H-decreasing branches. The H-increasing $M(H)$ curve consists of four well-separated magnetization steps. These multisteps might originate from magnetic field-induced transition between different PDA states or from quantum tunneling of the magnetization [20,21]. As temperature rises to 8 K, the hysteresis is much suppressed. Both the H-increasing and the H-decreasing $M(H)$ curves are characterized by a first magnetization step at 1/3 of magnetization saturation, followed by a second jump at 3.4 T which corresponds to the FIM–FM transition. In this FIM state, 2/3 of spin chains are ferromagnetically coupled and the left 1/3 points to the opposite direction, resulting in a net magnetization of only 1/3 of the saturation magnetization. Further increasing temperature to 13 K, this FIM step becomes ambiguous due to the thermal effect. As the Fe concentration increases, both the FIM step and the multisteps become less defined and almost disappear at $x = 0.7$. Meanwhile, the $M(H)$ curves becomes less hysteretic compared to that of $x = 0.2$. These observations are quite similar to those reported in the Cr- and Mn-doped compounds [13,17]. Thus, in the Fe-doped compounds, the FIM state can be suppressed by a breaking of FM coupling as well as a strengthening of AFM coupling within the spin chain. As far as the PDA state is concerned, it was proposed that creation of AFM defects along the chains by the Cr substitution could make the magnetic behavior closer to the PDA state [13]. This, together with the neutron diffraction data [16], makes us assume the presence of PDA state in the Fe-doped compounds. With this assumption, the FIM state observed in Fig. 5 is induced from the zero-field PDA state.

For $x = 1.1$ with triclinic phase (Fig. 5d), the magnetization is much smaller than that of $x \leq 0.7$. The magnetization at 2 K varies almost linearly with magnetic field, characterizing again the AFM state. The curves are hysteretic in low fields and present a slight upturn around 6 T. The $M(H)$ curves at 13 K ($>T_N = 7$ K) exhibit a PM-like behavior. The small deviation from a straight line as well as the small hysteresis may imply the presence of short-range FM clustering, in accord with the result of $M(T)$ curve (Fig. 3b).

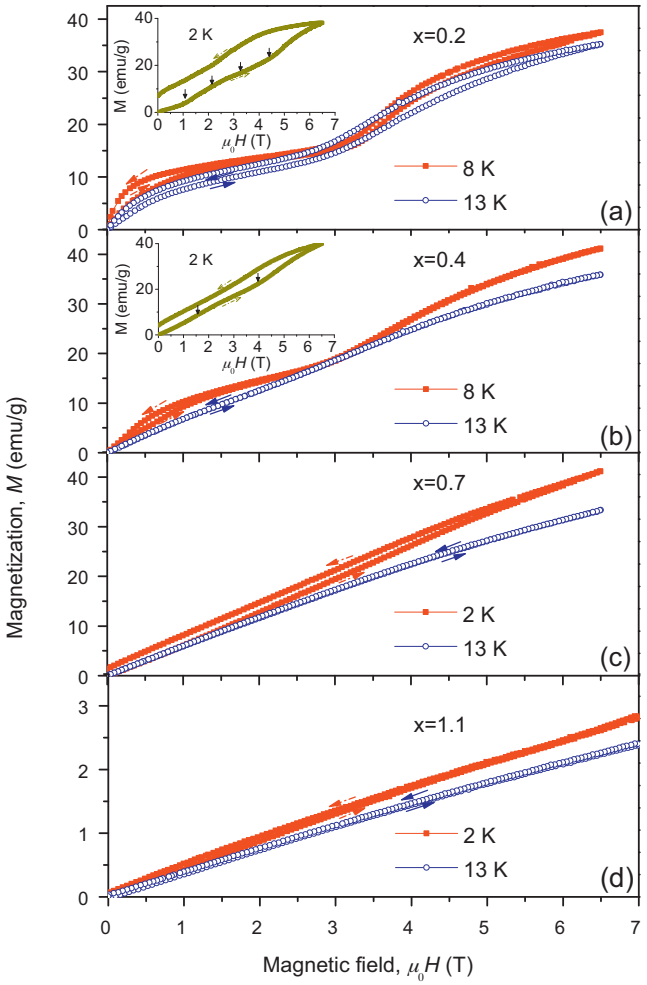

Fig. 5. $M(H)$ curves measured at several temperatures for $x = 0.2$, 0.4, 0.7 and 1.1. The vertical arrows point to the multisteps. The inclined arrows show the direction of magnetic field change.

3.3. ESR spectra

Fig. 6 plots the temperature dependence of the first-derivative ESR spectra of $x = 0.4$, which owns a pure rhombohedral phase compared to other Fe-doped compounds (see Fig. 1). No resonance is detected within 300–60 K. As temperature is lowered to be 50 K, a resonance consisting of eight hyperfine-structure peaks starts to emerge. Such hyperfine peaks, which become well defined with decreasing temperature, are due to the splitting produced by Co nuclei. The nuclear spin quantum number of ^{59}Co is I = 7/2 and a resonance superimposed with eight (2I + 1) hyperfine splittings is expected. No shift of the resonance is detected as temperature reduces. The corresponding g value is derived to be 4.2, much larger than 2.0. This again shows that observed resonance is due to Co ions with strong crystal-field effects of octahedra and trigonal prisms. It is worth noting that as temperature approaches to the ordering temperature of ~8 K, an additional peak marked by arrows in the figure appears. This peak becomes stronger in intensity and shifts towards lower field with decreasing temperature. At present, the origin for this additional resonance is unknown. Thus, our ESR spectra of $x = 0.4$ show that only resonance of Co ions is observed, different from the case of $Ca_3Co_{1.98}Fe_{0.02}O_6$ exhibiting strong impurity spin resonance of Fe^{3+} [18].

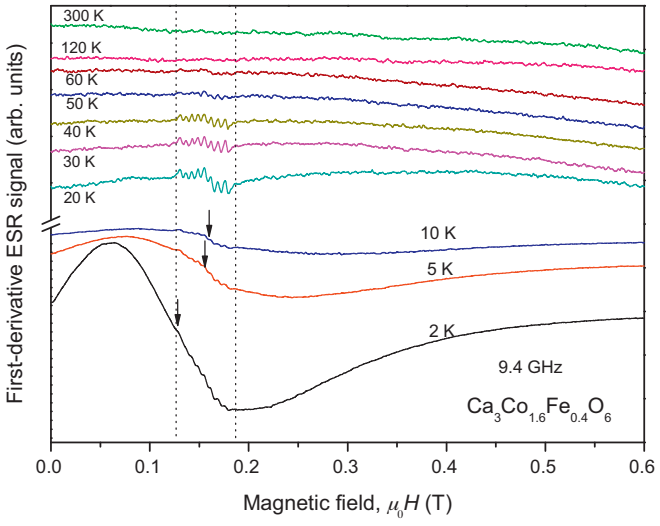

Fig. 6. Temperature dependence of the first-derivative ESR spectra of $x = 0.4$. The additional peak is shown by arrows.

4. Conclusions

In summary, room temperature XRD shows that samples with $x = 0$–0.7 crystallize in the rhombohedral structure ($R\bar{3}c$) and those with $x = 1.1$–1.5 have a triclinic structure ($P\bar{1}$). In the rhombohedral phase, the high-temperature H/M curve follows Curie–Weiss law, while the low-temperature part exhibits an upturn due to the presence of short-range ordering. Interestingly, this upturn tends to disappear and θ_P approaches zero at $x = 0.7$. A FIM sate with its magnetization being 1/3 of the saturation is observed for $x = 0.2$ and 0.4. This feature can be suppressed as the Fe concentration increases. The ESR spectra of $x = 0.4$ reveal a resonance of Co ions, which is superimposed with eight hyperfine structure peaks. For the triclinic compound with $x = 1.1$, the magnetization curves characterize the presence of AFM ground state. The H/M curve fails to follow the Curie–Weiss law, which might suggest that the ordering temperature is well above 300 K or short-range FM correlations exist in the PM matrix.

Acknowledgments

The authors thank W. Tong at High Magnetic Field Laboratory of the Chinese Academy of Sciences, China for providing help in ESR experiments. The work is supported by the National Natural Science Foundation of China (Grant No. 11074083) and Program for New Century Excellent Talents in University (NCET-10-0413).

References

[1] S. Aasland, H. Fjellvåg, B. Hauback, Solid State Commun. 101 (1997) 187.
[2] H. Kageyama, K. Yoshimura, K. Kosuge, J. Solid State Chem. 140 (1998) 14.
[3] S. Niitaka, K. Yoshimura, K. Kosuge, M. Nishi, K. Kakurai, Phys. Rev. B 87 (2001) 17.
[4] R. Frésard, C. Laschinger, T. Kopp, V. Eyert, Phys. Rev. B 69 (2004) 140405.
[5] S. Agrestini, C. Mazzoli, A. Bombardi, M.R. Lees, Phys. Rev. B 77 (2008) 140403.
[6] P.L. Paulose, N. Mohapatra, E.V. Sampathkumaran, Phys. Rev. B 77 (2008) 172403.
[7] K. Mukherjee, E.V. Sampathkumaran, J. Alloys Compd. 498 (2010) 1.
[8] H. Fjellvåg, E. Gulbrandsen, S. Aasland, A. Olsen, B.C. Hauback, J. Solid State Chem. 124 (1996) 190.
[9] H. Kageyama, K. Yoshimura, K. Kosuge, H. Mitamura, T. Goto, J. Phys. Soc. Jpn. 66 (1997) 1607.
[10] P.L. Li, X.Y. Yao, F. Gao, C. Zhao, K.B. Yin, Y.Y. Weng, J.-M. Liu, Z.F. Ren, Appl. Phys. Lett. 91 (2007) 042505.
[11] C.H. Hervoches, V.M. Fredenborg, A. Kjekshus, H. Fjellvåg, B.C. Hauback, J. Solid State Chem. 180 (2007) 834.
[12] V.G. Zubkov, G.V. Bazuev, A.P. Tyutyunnik, I.F. Berger, J. Solid State Chem. 160 (2001) 293.

[13] D. Flahaut, A. Maignan, S. Hébert, C. Martin, R. Retoux, V. Hardy, Phys. Rev. B 70 (2004) 094418.
[14] A. Jain, S. Singh, S.M. Yusuf, Phys. Rev. B 74 (2006) 174419.
[15] I. Nowik, A. Jain, S.M. Yusuf, J.V. Yakhmi, Phys. Rev. B 77 (2008) 054403.
[16] A. Jain, S.M. Yusuf, J. Campo, L. Keller, Phys. Rev. B 79 (2009) 184428.
[17] C.H. Hervoches, H. Okamoto, A. Kjekshus, H. Fjellvåg, B.C. Hauback, J. Solid State Chem. 182 (2009) 331.
[18] H. Kageyama, K. Yoshimura, K. Kosuge, H. Nojiri, K. Owari, M. Motokawa, Phys. Rev. B 58 (2009) 17.
[19] A. Maignan, V. Hardy, S. Hébert, M. Drillon, M.R. Lees, O. Petrenko, D.McK. Paul, D. Khomskii, J. Mater. Chem. 14 (2004) 1231.
[20] T. Takagi, M. Mekata, J. Phys. Soc. Jpn. 64 (1995) 4609.
[21] V. Hardy, D. Flahaut, M.R. Lees, O.A. Petrenko, Phys. Rev. B 70 (2004) 214439.